Theoretical Electron Density Distributions for Fe- and Cu-Sulfide Earth Materials: A Connection between Bond Length, Bond Critical Point Properties, Local Energy Densities, and Bonded Interactions

G. V. Gibbs,*,† D. F. Cox,‡ K. M. Rosso,§ N. L. Ross,† R. T. Downs,|| and M. A. Spackman⊥

Department of Geosciences, and Department of Chemical Engineering, Virginia Tech, Blacksburg, Virginia 24061, William R. Wiley Environmental Molecular Sciences Laboratory, Pacific Northwest National Laboratories, Richland, Washington 99352, Department of Geosciences, University of Arizona, Tucson, Arizona 85721, and School of Biomedical, Biomolecular and Chemical Sciences, University of Western Australia, Australia

Received: August 7, 2006; In Final Form: December 6, 2006

Bond critical point and local energy density properties together with net atomic charges were calculated for theoretical electron density distributions, $\rho(\mathbf{r})$, generated for a variety of Fe and Cu metal-sulfide materials with high- and low-spin Fe atoms in octahedral coordination and high-spin Fe atoms in tetrahedral coordination. The electron density, $\rho(\mathbf{r}_c)$, the Laplacian, $\nabla^2\rho(\mathbf{r}_c)$, the local kinetic energy, $G(\mathbf{r}_c)$, and the oxidation state of Fe increase as the local potential energy density, $V(\mathbf{r}_c)$, the Fe−S bond lengths, and the coordination numbers of the Fe atoms decrease. The properties of the bonded interactions for the octahedrally coordinated low-spin Fe atoms for pyrite and marcasite are distinct from those for high-spin Fe atoms for troilite, smythite, and greigite. The Fe−S bond lengths are shorter and the values of $\rho(\mathbf{r}_c)$ and $\nabla^2\rho(\mathbf{r}_c)$ are larger for pyrite and marcasite, indicating that the accumulation and local concentration of $\rho(\mathbf{r})$ in the internuclear region are greater than those involving the longer, high-spin Fe−S bonded interactions. The net atomic charges and the bonded radii calculated for the Fe and S atoms in pyrite and marcasite are also smaller than those for sulfides with high-spin octahedrally coordinated Fe atoms. Collectively, the Fe−S interactions are indicated to be intermediate in character with the low-spin Fe−S interactions having greater shared character than the high-spin interactions. The bond lengths observed for chalcopyrite together with the calculated bond critical point properties are consistent with the formula $Cu^{+}Fe^{3+}S_2$. The bond length is shorter and the $\rho(\mathbf{r}_c)$ value is larger for the FeS_4 tetrahedron displayed by metastable greigite than those displayed by chalcopyrite and cubanite, consistent with a proposal that the Fe atom in greigite is tetravalent. S−S bond paths exist between each of the surface S atoms of adjacent slabs of FeS_6 octahedra comprising the layer sulfide smythite, suggesting that the neutral Fe_3S_4 slabs are linked together and stabilized by the pathways of electron density comprising S−S bonded interactions. Such interactions not only exist between the S atoms for adjacent S_8 rings in native sulfur, but their bond critical point properties are similar to those displayed by the metal sulfides.

Introduction

Transition metal sulfides are an important class of Earth materials that display a fascinating assortment of bonded interactions and structure types in concert with a host of important electronic, magnetic, and catalytic properties.[1−5] Sulfides are also important economic and industrial staples for mankind, providing the main resources for the bulk of the world supplies of non-ferrous metals. The properties have attracted the attention of chemists, material scientists, physicists, and mineralogists alike who have undertaken a relatively wide variety of experimental and theoretical studies, resulting in the invention of sulfide-based catalysts, magnetic sensors, solar cell materials, solid-state batteries, and lubricants, among other things.

In a historical perspective presented 25 years ago at Castle Hot Springs, AZ, Linus Pauling[6] reminisced about his early days at Caltech when he "...considered sulfides to be a pretty interesting field." He went on to say that "I thought that I knew all about the silicates by that time, but I did not understand sulfides at all and I thought that we ought to be determining a lot of sulfide structures." Intent on attacking and resolving this important problem, Pauling approached the Geological Society of America with a proposal requesting a $3000 Penrose Grant to study sulfides with the goal of formulating a new set of rules for determining their structures comparable to those that he had formulated for complex silicate crystals, rules that have since provided an important underpinning for much of our understanding of silicate crystal chemistry. Several months later, he received a letter of rejection with the silly comment "...that perhaps this was not geology." Undaunted, Pauling resubmitted his application, explaining "...to the old geologist at MIT why it was important to do this sort of work." He never heard back, an outcome that was clearly a material setback for understanding sulfide crystal chemistry.

One can appreciate the challenging problems that confronted Pauling in understanding sulfides given their structural and chemical complexities, as compared with those displayed by

* Corresponding author. E-mail: gvgibbs@vt.edu.
† Department of Geosciences, Virginia Tech.
‡ Department of Chemical Engineering, Virginia Tech.
§ Pacific Northwest National Laboratories.
|| University of Arizona.
⊥ University of Western Australia.

10.1021/jp065086i CCC: $37.00
Published on Web 02/03/2007

silicates. For example, metal excess sulfides display non-stoichiometric formulas like Ni_7S_6 that do not appear to be charge balanced, a class of formulas unknown for silicates. Silicates are only known to contain metal−oxygen (M−O) bonded interactions, and their structures are often comparatively less complicated, consisting of 3D arrays of corner-, edge-, and, in some cases, face-sharing MO_n coordinated polyhedra. Sulfides also consist of corner-, edge,- and face-sharing MS_n coordinated polyhedra, but, in sharp contrast, the transition metal M atoms for a number are not only bonded to S, but they are also bonded to the M atoms in adjacent coordinated polyhedra such as three MS_4 tetrahedra sharing a common edge.[7−9] Another complication is that some contain S_2 dimers,[1,4] suggesting the possibility that S−S bonded interactions may be present in other sulfides. In contrast, dioxide O_2 dimers are unknown to us in silicates. A short O−O contact (2.11 Å) has been reported in a high-pressure structure determination of a silica polymorph with the pyrite structure, but, despite the presence of a well-developed bond path connecting the O atoms, the lack of maxima in the electron localization function maps along the O−O vector was asserted to indicate that the O atoms are nonbonded.[10]

Assuredly, the presence of M−M and S−S bonded interactions contributes to the complexities of the sulfide structures and underlies the occurrence of non-stoichiometric chemical formulas as observed above.[1,2,7,9] These interactions present a problem in the consideration of bond valences and bond valence sums as embodied in Pauling's rules[11] (particularly his second rule).[2,4,7,9] Nonetheless, for Fe sulfides lacking Fe−Fe and S−S bonded interactions, Hoggins and Steinfink[12] established a bond valence−bond length connection for a variety of Fe−S bonded interactions, similar to that established for the M−O bonded interaction derived for oxides.[13] With this connection, they not only found that the valence of Fe correlates with Mössbauer isomer shifts and electrical conductivity, but that it also provides a strategy for estimating the oxidation state of Fe.

With the advent of the single-crystal diffractometer, new X-ray sources of radiation, and the computer during the middle and late last century, it is not surprising that the crystal structures of a large number of silicates were determined and that material gains were made in developing an experimental and theoretical basis for understanding silicate crystal chemistry.[8,13−17] Substantially less gain was made for sulfides due in large part to the common presence of crystal defects such as twinning, zoning, exsolution, and disorder. Electron density distributions, bond critical point, and the local energy density properties calculated for a relatively large number of oxides and silicates have been found to be in adequate agreement with those determined experimentally with accurate high resolution and high-energy synchrotron experimental diffraction data, whereas, to our knowledge, few such studies have been completed for sulfides.[8]

A notable exception is the careful study of the spin of nominally divalent Fe undertaken by Stevens et al.,[18] who completed a mapping of the experimental deformation electron density distribution, $\Delta\rho(\mathbf{r})$, for pyrite, FeS_2, to establish a connection between the distribution and the crystal field splitting of the d-orbitals on the Fe atom. They found that static $\Delta\rho(\mathbf{r})$ maps display eight peaks between 1.2 and 1.6 e/Å^3 in height at ∼0.6 Å from the Fe atom directed toward the faces of the FeS_6 octahedron, as expected for a $(t_{2g})^6(e_g)^0$ low-spin configuration and suggested by paramagnetic susceptibility[19] and Mössbauer measurements.[4,20] A slight trigonal distortion of the octahedron was found to result in a splitting of the three degenerate t_{2g} energy levels into a_g and e_g levels. Further, the d-orbital populations determined in multipole refinements of $\rho(\mathbf{r})$ were not only found to be significantly different from the values expected for a spherical high-spin divalent Fe atom but to yield an occupancy of 2.0 for the a_g orbital in exact agreement with the value of 2.0 expected for low-spin divalent Fe. Using the parameters obtained in the multipole refinement, they were also successful in the calculation of the electric field gradient at the Fe nucleus together with the magnitude of the quadrupole splitting of the Mössbauer spectra. Deformation maps generated in a theoretical study of pyrite have since been found to be consistent in large part with the experimental maps showing peaks radiating from Fe in the directions of the octahedral faces,[21] demonstrating that experimental deformation maps can be useful in the study of bonded interactions despite the well-known fact that a procrystal representation of $\rho(\mathbf{r})$ is not unique. In a study of the connection between the electron density, ED, distributions for a number of pyrite structure types, and the catalytic activity in hydrodesulfurization (HDS), Aray et al.[22,23] calculated the bond critical point, bcp, properties for a number of transition metal disulfides, finding bond paths between M atoms and S and between the S atoms of the S_2 dimers. They also found that the HDS catalytic activity is connected to the chemical character of the transition metal involved in the adsorption process. The calculation for pyrite yielded a $\rho(\mathbf{r}_c)$ value of 0.55 e/Å^3 for the Fe−S bonded interaction and a larger value of 0.89 e/Å^3 for the S−S interaction, values that are in exact agreement with those calculated in this study.

The bond critical point and the local density properties were recently calculated for the theoretical ED distributions for three Ni-sulfides vaesite (NiS_2), millerite (NiS), and heazlewoodite (Ni_3S_2) and for bulk Ni metal.[7] The study revealed that bond paths not only exist between the Ni and S atoms, but that they also exist between adjacent Ni atoms. As the Ni−Ni separations and the bcp properties for the separations in millerite and heazlewoodite (2.50−2.53 Å) closely match those calculated for bulk Ni metal (2.49 Å), it was concluded that the Ni atoms are bonded like those in bulk Ni metal.[24] Accordingly, the ED associated with the Ni−Ni bond paths was asserted to stabilize the structures of millerite and heazlewoodite[9] beyond that of the stabilizing Fe−S bonded interactions. The net atomic charges conferred on the Ni and S atoms in vaesite and millerite were found to be a fraction of the formal valences of the atoms with the net charge on Ni decreasing with decreasing Ni−S bond length. Smaller net charges were likewise calculated for the Ni atoms in Ni excess heazlewoodite that were related to its Ni−Ni bonded interactions, its metallic character, and to the greater shared character of its bonded interactions. The local kinetic, potential, and electronic energy density properties and the bcp properties indicate that the Ni−S and Ni−Ni interactions are intermediate in character between closed-shell and shared interactions. It was also observed that the high metallic conductivity and the delocalization of the electrons in heazlewoodite are consistent with its well-developed and robust metallic band structure.[25] In addition, the metallic conductivity was related to the presence of four well-developed Ni−Ni bond paths that radiate from each Ni atom, connecting the Ni atoms in the structure into a highly branched continuous circuit of interconnected Ni−Ni bond paths. The end product is a crystal that can be pictured as wired with Ni−Ni bond paths of accumulated ED that radiate throughout the crystal, ideally suited for electron transport. The non-stoichiometic formula for heazelewoodite suggests that the oxidation state of the Ni atoms is intermediate between Ni^+ and Ni^{2+}. In a previous study of the electronic structure for two Ni bearing dipyridylamide

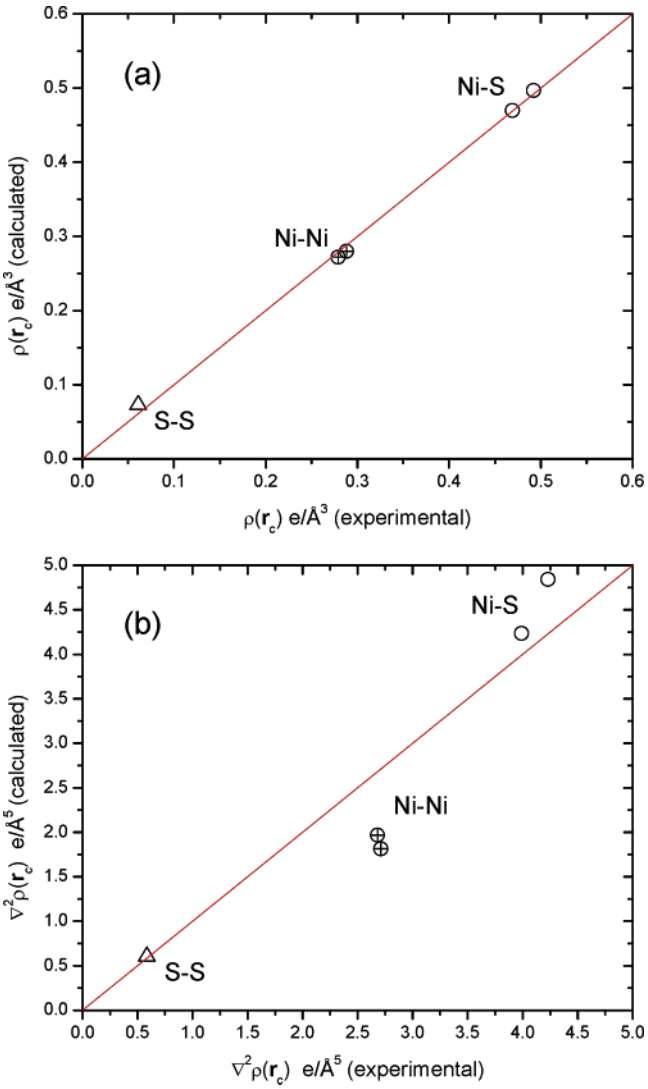

Figure 1. A comparison of the experimental and theoretical electron density, $\rho(\mathbf{r}_c)$ (a), and the Laplacian of $\rho(\mathbf{r}_c)$, $\nabla^2\rho(\mathbf{r}_c)$, values (b) for heazlewoodite, Ni_3S_2, each determined at the (3,−1) bond critical points for the Ni−S, Ni−Ni, and S−S bonded interactions.[7,27] The Ni−S bonded interactions are plotted as ○, the Ni−Ni interactions are plotted as ⊕, and the S−S interactions are plotted as △. The data are compared with an ideal line with a 45° slope.

molecules with Ni−Ni separations measuring ~2.45 Å, Ni metallic wires were likewise pictured by Kiehl at al.[26] as potential circuits for electron transport.

This Study

An accurate set of high-resolution single-crystal X-ray diffraction data was recently collected, and a conventional multipole refinement and modeling of the experimental ED distribution was completed for a synthetic heazlewoodite crystal.[27] A generation of the bcp properties for the distribution revealed that each of the bond paths displayed by the theoretical distribution is faithfully displayed by an experimental path. The values of the theoretical ED, $\rho(\mathbf{r}_c)$, evaluated at the bond critical points, $\mathbf{r}_c$, are compared with the experimental values in Figure 1a where the experimental values for the Ni−S, Ni−Ni, and S−S interactions are seen to be in good agreement with the theoretical values. The experimental values for the Laplacian, $\nabla^2\rho(\mathbf{r}_c)$, for the Ni−S and S−S interaction are also in good agreement with the theoretical values (Figure 1b), but the experimental values for the Ni−Ni interactions depart from the

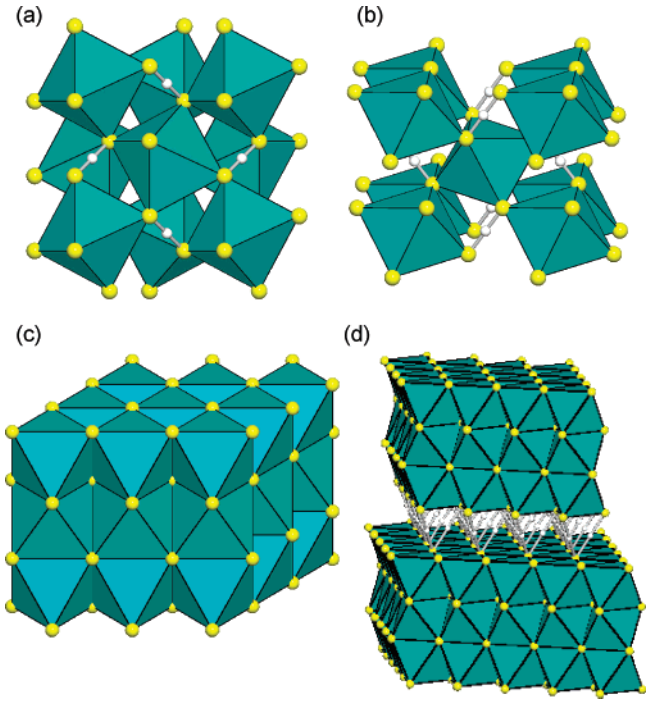

Figure 2. Drawings of the crystal structures for pyrite, FeS_2 (a), marcasite, FeS_2 (b), troilite, FeS (c), and smythite, Fe_3S_4 (d). The green octahedra house Fe atoms, and the yellow spheres represent the S atoms. The octahedra of pyrite and marcasite are linked together by S_2 dimers into a framework of corner-sharing FeS_6 octahedra. The S_2 dimers are connected by bond paths displayed by gray straight lines. The small white spheres represent the (3,−1) bond critical points for the S−S bonded interaction. The sulfur atoms comprising the surfaces of the slabs of the smythite structure are also connected by bond paths each with a bcp point, three of which radiate from each S atom.

trend and are ~0.5 e/Å^5 larger than those calculated. Given that the Laplacian is the second derivative of the ED, poorer agreement may be anticipated. Nonetheless, the quality of the diffraction data and the modeling of the experimental distribution are considered to be adequate in that the experimental properties are in reasonably good agreement with the theoretical ones.[28] Encouraged by the agreement, we have completed similar calculations for the Fe−S, Fe−Fe, and S−S bonded interactions comprising the Fe-sulfides pyrite (FeS_2), marcasite (FeS_2,) troilite (FeS), smythite (Fe_3S_4), and greigite (Fe_3S_4), and the Fe−Cu-sulfides chalcopyrite ($CuFeS_4$) and cubanite ($Cu\ Fe_2S_3$).

Crystal Structures

The crystal structures of the disulfides pyrite and marcasite consist of corner-sharing FeS_6 octahedra linked together by S_2 dimers where each S atom of a dimer defines the corner shared in common by three octahedra (Figure 2a,b). However, unlike the FeS_6 octahedra in pyrite, which only share corners, each of the octahedra in marcasite also shares two edges with adjacent octahedra, forming chains of edge-sharing octahedra running parallel to the *c*-cell edge vector **c** (Figure 2b). Like pyrite and marcasite, troilite and smythite also consist of corner-sharing FeS_6 octahedra, but, unlike pyrite and marcasite, they are linked together by single S atoms rather than by S_2 dimers. Also, unlike pyrite and marcasite with low-spin Fe atoms, the Fe atoms in troilite and smythite are in the high-spin state. The S atoms in troilite can be viewed as hexagonal close-packed (hcp) with one-half of the available octahedral voids occupied by nominally divalent Fe. As such, each FeS_6 octahedron shares faces with two adjacent antipodal FeS_6 octahedra with the remaining edges

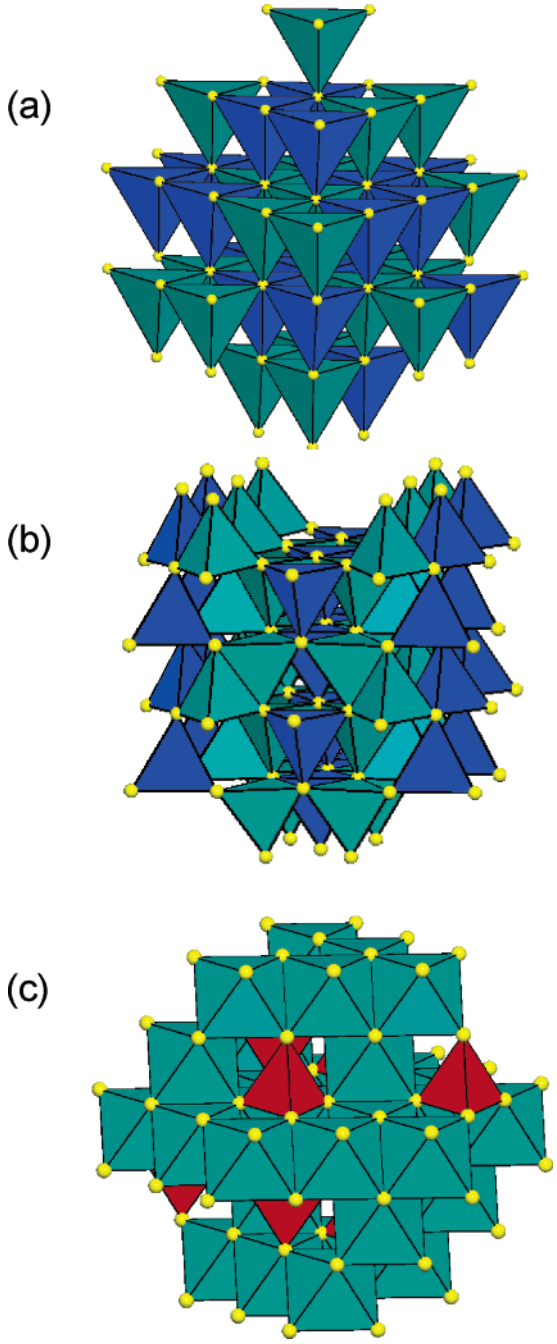

Figure 3. Drawings of the crystal structures for chalcopyrite, $CuFeS_2$ (a), cubanite, $CuFe_2S_3$ (b), and greigite, Fe_3S_4 (c). The blue and green tetrahedral house Cu and Fe atoms, and the green octahedral and red tetrahedral house Fe, respectively. The yellow spheres represent S atoms.

shared by FeS_6 octahedra (Figure 2c). Unlike troilite, smythite is a sheet structure that consists of a succession of parallel slabs of FeS_6 octahedra each separated ~3.5 Å apart (Figure 2d). The slabs have the troilite structure and consist of three layers of face-sharing FeS_6 octahedra. The Fe−S bond length vectors that radiate to the surface S atoms of the slabs are shorter, 2.42 Å, than those involving the interior Fe−S bond length vectors (2.46 Å), as may be expected from local valence balance considerations.[12]

In contrast, the structures of chalcopyrite and cubanite each consist of FeS_4 and CuS_4 corner-sharing tetrahedra (Figure 3a and b, respectively). In the case of chalcopyrite, the structure can be described as a cubic close-packed (ccp) array of S atoms in which one-eighth of the available tetrahedral voids are occupied by high-spin nominally trivalent Fe atoms and one-eighth are occupied by nominally monovalent Cu atoms such that each S atom is bonded to two Fe and two Cu atoms.[29,30] The Fe−S bond length observed for chalcopyrite (2.26 Å)[31] is in exact agreement with that generated with Shannon's[32] crystal radii (2.26 Å) for nominally trivalent high-spin tetrahedrally coordinated Fe. The observed Cu−S bond length (2.30 Å) is also in agreement with that generated with Shannon radii (2.33 Å).[32] The agreement is consistent with the conclusion that one of the two nonequivalent tetrahedra in chalcopyrite is occupied by a high-spin nominally trivalent Fe atom and the other by a monovalent Cu atom, resulting in the $Cu^+Fe^{3+}S_2$ formula.[30] The valence strength−bond length connection yields an oxidation number for the Fe atom of 2.79, 10% smaller than that observed for chalcopyrite.[12]

In contrast, the cubanite structure can be described as an hcp array of S atoms where one-sixth of the available tetrahedral voids are occupied by nominally monovalent Cu atoms and one-third are occupied by Fe atoms. Unlike the chalcopyrite structure where the FeS_4 tetrahedra only share corners, the tetrahedra in cubanite each share one edge in forming pairs of edge-sharing tetrahedra. As the nominal valence of the Cu atom is one, it has been asserted that each tetrahedral pair contains a random distribution of Fe^{2+} and Fe^{3+} atoms as evinced by neutron diffraction and Mössbauer data that show that these two edge-sharing FeS_4 tetrahedra are inversion center equivalent in agreement with a random distribution of atoms.[9,33,34] As such, McCammon et al.[35] have concluded that the valences of the Fe atoms represent a rapid electron transfer of delocalized electrons between Fe^{2+} and Fe^{3+} as proposed for the octahedra of greigite (see below). The average Fe−S bond length observed for the tetrahedra in cubanite is 2.275 Å, slightly larger than that generated (2.255 Å) for a Fe^{3+}−S bond length with Shannon's radii[32] but smaller than that generated for a random distribution of Fe^{2+} and Fe^{3+} (2.308 Å). In contrast, the average bond length observed for the CuS_4 tetrahedron, 2.305 Å, is statistically identical to that observed for chalcopyrite, 2.302 Å.

The rms amplitudes of the thermal ellipsoid observed for the random arrangement of Fe atoms in cubanite (0.108 Å) are substantially smaller, on average, than those observed for the ordered Cu atoms (0.137 Å).[35] Also, given that the Hoggins−Steinfink estimate of the Fe valence for cubanite is slightly smaller (2.77) than that estimated for chalcopyrite[12] (2.79) and that the average ^{IV}Fe−S bond length observed for cubanite is slightly longer than that observed for chalcopyrite, collectively the evidence suggests that the Fe atoms in the pair of tetrahedra behave as a single atom with a given oxidation state as suggested by Fleet[36] rather than a random distribution of Fe^{2+} and Fe^{3+}. It is noteworthy that the presence of an Fe atom with the same oxidation state is consistent with the time scale of the Mössbauer effect. A recent study of the equation of state, the bond character, and Mössbauer data collected at high pressures also indicates a single Fe atom with an intermediate oxidation state between Fe^{2+} and Fe^{3+}.[37] However, if Fe^{2+} and Fe^{3+} are randomly distributed between the pair of tetrahedra, then the rms amplitudes for the Fe atoms would be expected to be substantially larger than that observed for the Cu atom, which is not the case.[35]

Unlike the previous structures, greigite (Figure 3c) is generally believed to consist of both tetrahedrally and octahedrally coordinated Fe atoms comprising the inverse spinel structure with the formula $Fe^{3+}(Fe^{2+}Fe^{3+})S_4$.[38,39] As is well known, greigite is metastable, which accounts for its rarity in nature and its difficult synthesis.[4] The structure can be described as a

ccp array of S atoms with Fe^{3+} occupying one-eighth of the available tetrahedral voids and $Fe^{2+}$and Fe^{3+} randomly distributed over one-half of the available octahedral voids. Its semimetallic character has been ascribed to the presence of nonstoichiometic Fe vacancies with electron hopping inferred to occur between high-spin Fe^{2+} and Fe^{3+} atoms in the octahedral voids. Using the Fe−S bond valence−bond length connection, it has been suggested that the tetrahedrally coordinated Fe atom in greigite is tetravalent rather than trivalent as assumed above. As found by Hoggins and Steinfink,[12] the connection yields a valence of 3.92 for the 4-coordinated Fe atom of greigite, close to an oxidation state of 4+. Further, Shannon[32] found that the connection yields a tetrahedral Fe^{4+}−S bond length of 2.144 Å, close to the experimental tetrahedral bond length, 2.147 Å, for greigite.[38] While Fe is known to exist in a tetravalent state, the Fe^{4+} cation is relatively rare and not particularly stable. Indeed, Hoggins and Steinfink[12] were careful to point out that it was very unlikely that the Fe atom is tetravalent. Moreover, Hong and Steinfink[40] concluded on the basis of a Mössbauer isomer shift of 0.17 mm/s and a magnetic susceptibility of 5.81 μ_B that the Fe atom in Ba_3FeS_5 is trivalent rather than tetravalent as indicated by its formula. The charge on the Fe atoms was considered to be reduced by a back-donation of an electron from the S to the Fe atom with a resulting Fe−S bond length, 2.24 Å, that is slightly shorter than that for a $^{IV}Fe^{3+}$−S bonded interaction, 2.25 Å.[41,42] Nonetheless, given the possibility that Fe is tetravalent in greigite and the possibility that the Fe atom in cubanite has an effective charge intermediate between Fe^{2+} and Fe^{3+}, it will be of interest to compare their bcp and local density properties with those calculated for chalcopyrite where the oxidation state of the Fe atom is known to be trivalent.[29,30]

Computational Details

Given the close agreement of the theoretical and experimental bcp properties reported for heazlewoodite, ED distributions were calculated and the bcp and the local energy density properties were calculated with the programs CRYSTAL98[43] and TOPOND[44] for the Fe-sulfides troilite,[45] pyrite,[18,20,46] marcasite,[47] chalcopyrite,[31] cubanite,[34,37] greigite,[38] and smythite.[48] The electronic structure for each crystal was computed with CRYSTAL98, using Bloch functions expanded as linear combinations of atomic centered Gaussian basis sets. Self-consistent field wave functions, solved in reciprocal space, were computed for each structure at the density functional theory level using the local density approximation formulated with the local spin density approximation for the exchange potential[49] and the Vosko−Wilk−Nusair[50] parametrization of the correlation potential. The basis sets used in the calculations were specifically optimized for use in the CRYSTAL98 program. For Fe and Cu, 86-411(d41)G basis sets optimized by Towler et al.[51] were used, and, for S, an 86-311G* basis set optimized by Lichanot et al.[52] was used. The bcp and the local energy density properties were computed using parameters described earlier[7] with the TOPOND[44] software.

Connection between the Experimental Fe−S Bond Lengths and the Theoretical Bond Critical Point Properties

The $\rho(\mathbf{r}_c)$ values calculated for the Fe sulfides, plotted against the observed Fe−S bond length, R(Fe−S) (Figure 4a), increase nonlinearly with the shorter bonded interactions involving larger values of $\rho(\mathbf{r}_c)$, a connection that has been reported for a relatively large number of different M−O bonded interactions and materials. As the coordination number of the Fe atom decreases from six for troilite, smythite, and greigite to four for cubanite, chalcopyrite, and greigite, R(Fe−S) decreases nonlinearly as defined by the dashed line. Also, the oxidation state of the Fe atom in the series is indicated to increase from 2+ to 3+ to 4+ if the oxidation state is intermediate between Fe^{2+} and Fe^{3+} in cubanite and Fe^{4+} in greigite. The experimental Fe−S bond lengths are slightly shorter, and the calculated $\rho(\mathbf{r}_c)$ values are slightly larger for chalcopyrite,[12,32] than those for cubanite, as may be expected if the oxidation state of the Fe atom in the latter is intermediate between Fe^{2+} and Fe^{3+}. The two nonequivalent bond lengths of cubanite involved in the shared edge are longer than those observed for chalcopyrite (2.26 Å), whereas those involved in the unshared edges are about the same as that observed for chalcopyrite with the average bond length (2.28 Å) for cubanite being slightly longer than that observed for chalcopyrite. The $\rho(\mathbf{r}_c)$ values calculated for the tetrahedral Fe−S bond in greigite (0.73 e/Å^3) are substantially larger than those calculated for cubanite (0.49 e/Å^3) and chalcopyrite (0.48 e/Å^3). The larger value of $\rho(\mathbf{r}_c)$ is expect if the oxidation state of the tetrahedrally coordinated Fe in greigite is nominally 4+.

As reported above, the Fe−S bond lengths observed for pyrite and marcasite with low-spin nominally divalent Fe atoms are substantially shorter (∼0.25 Å)[32] than those observed for the six-coordinate nominally divalent high-spin Fe atoms in troilite, greigite, and smythite.[2] Further, the bond lengths for the two disulfide polymorphs fall off the dashed curve in Figure 4a with their $\rho(\mathbf{r}_c)$ values ∼0.15 e/Å^3 larger than those calculated for the sulfides with 6-coordinate high-spin nominally divalent Fe. The bcp properties calculated for pyrite are in exact agreement with those calculated earlier by Aray et al.[22,23]

A recent study of the bcp properties calculated for the Si−O bonded interactions for silicate crystals and representative hydroxyacid silicate molecules demonstrates that the geometry and the properties calculated for the molecules match those calculated and observed for the crystals.[53] Given this agreement, the structure of the H_4FeS_4 molecule (S_4 point symmetry and tetravalent Fe^{4+}) was geometry optimized at the B3LYP/6-311++(2d,p) level for purposes of comparing the optimized ^{IV}Fe−S bond length with that observed for greigite. The calculation resulted in a Fe−S bond length of 2.130 Å, slightly shorter than that observed for greigite (2.147 Å). Using the software EXTREME, kindly provided by Professor Richard Bader, the bcp properties were calculated. Although the Fe−S bond length is slightly shorter than that observed for greigite, the value of $\rho(\mathbf{r}_c)$ (0.73 e/Å^3) for the Fe−S bonded interaction for the molecule matches that calculated for greigite exactly (Figure 4a).

Figure 4b shows that $\nabla^2\rho(\mathbf{r}_c)$ also increases in value with the decreasing bond length, the oxidation state, and the coordination number for the Fe atom. Also, the $\nabla^2\rho(\mathbf{r}_c)$ values for pyrite and marcasite are ∼0.2 e/Å^5 larger than those calculated for the sulfides with 6-coordinate nominally divalent high-spin Fe atoms. Clearly, the Fe−S bonded interactions involving low-spin Fe atoms are distinct from those displayed by the high-spin Fe atoms with a greater accumulation and local concentration of $\rho(\mathbf{r})$ in the bcp regions of the Fe−S bonded interactions and shorter bond lengths as compared with those involving the high-spin Fe atoms in troilite and smythite. The $\nabla^2\rho(\mathbf{r}_c)$ values for chalcopyrite and cubanite are similar (4.07−4.24 e/Å^5), but they are substantially smaller than that calculated for greigite (4.88 e/Å^5). However, they are also smaller than the value calculated for the H_4FeS_4 molecule (4.30 e/Å^5). Unlike

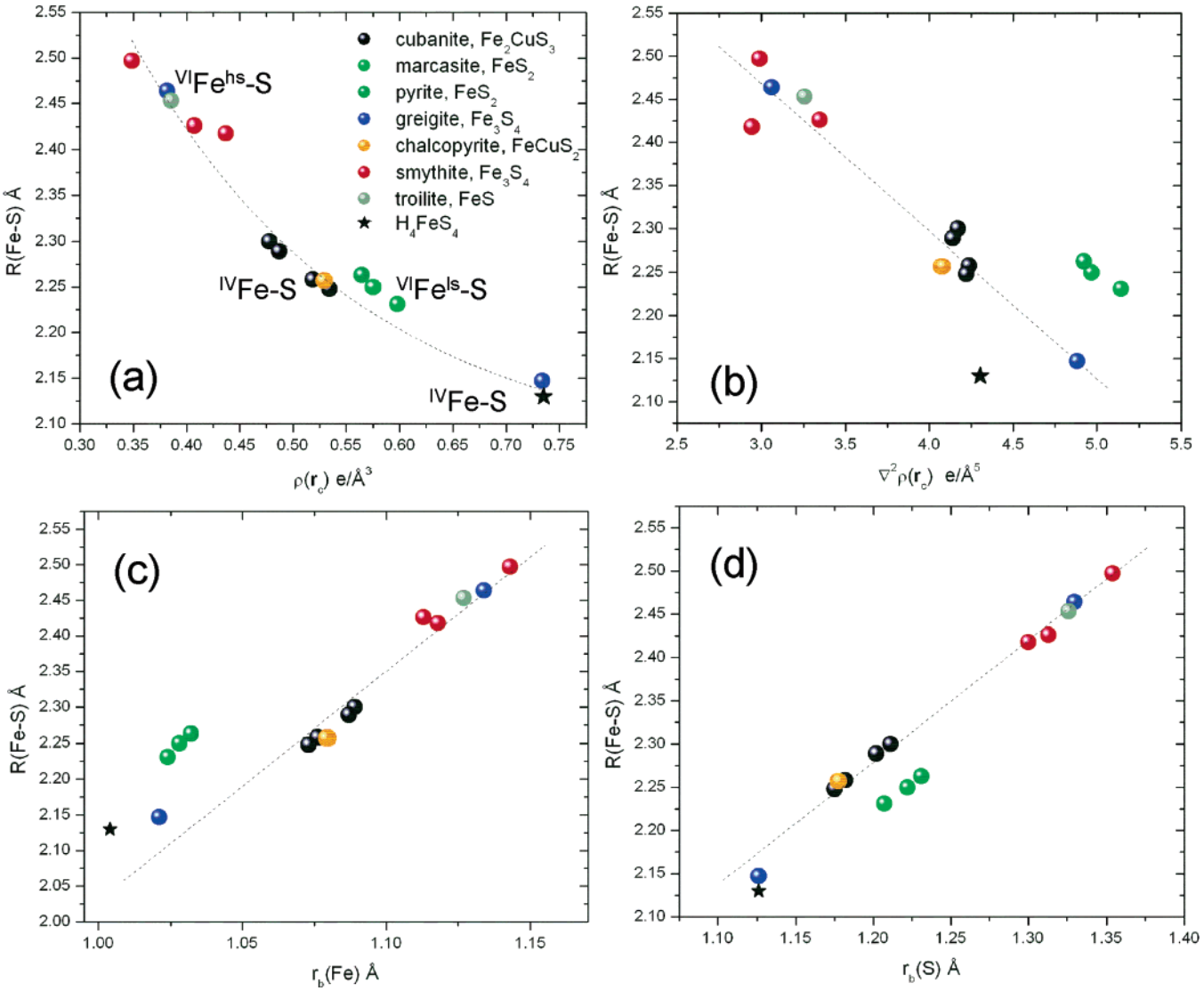

Figure 4. The experimental bond lengths, R(Fe−S), for the color coded sulfide data displayed in the upper right corner of (a) plotted against the calculated value of electron density, $\rho(\mathbf{r}_c)$ e/Å^3 (a), the Laplacian of $\rho(\mathbf{r}_c)$ e/Å,[5] $\nabla^2\rho(\mathbf{r}_c)$ (b), the bonded radii of Fe, r_b(Fe) Å (c), and the bonded radius of S, r_b(S) Å (d), each evaluated at bond critical points.

the close agreement of the $\rho(\mathbf{r}_c)$ value, $\nabla^2\rho(\mathbf{r}_c)$ for greigite is somewhat larger, ∼15%, than that calculated for H_4FeS_4 molecule.

In the calculations, no bond paths were found between the adjacent Fe atoms as reported earlier between the Ni atoms in heazlewoodite and millerite.[7] As such, evidence is lacking for Fe−Fe bonded interactions in troilite, smythite, and cubanite. Consistent with this result, the Fe−Fe separations between the Fe atoms in the face-sharing octahedra in smythite (2.86 Å) and troilite (2.90 Å) and the edge-sharing tetrahedra in cubanite (2.80 Å) are substantially longer than that displayed by bulk Fe metal (2.48 Å). The Fe−Fe separations are also substantially longer than those (2.73 Å) between the edge-sharing FeS_4 tetrahedra in $Ba_{13}Fe_7S_{25}$ where a delocalization of electrons is asserted to take place in the reduction of the charges on the Fe atoms (ref 42). The Ni−Ni separations in the Ni-sulfides heazlewoodite and millerite are very similar to those in bulk Ni metal with Ni−Ni bond paths resulting between the Ni atoms in both the sulfides and the metal that exhibit the same exact properties. However, well-developed bond paths were found to exist between the S_2 dimers in pyrite and marcasite (Figure 2a,b).

As displayed in Figure 4c and d, the bonded radii of the Fe and S atoms, r_b(Fe) and r_b(S), decrease linearly in size with decreasing R(Fe−S) with the radii for marcasite and pyrite (low-spin) again falling along one trend while those for the remaining sulfides (high-spin) fall along another. As expected, the bonded radii of the Fe atoms comprising the FeS_6 octahedra in troilite, smythite, and greigite are larger than those comprising the FeS_4 tetrahedra in chalcopyrite, cubanite, and greigite. Also, the bonded radii of the low-spin divalent Fe atoms in pyrite and marcasite are ∼0.1 Å smaller than the high-spin divalent Fe atoms of troilite, smythite, and greigite. Thus, the shorter low-spin Fe−S bond lengths depend on the radii of both the Fe and S atoms rather than just on the radius of the Fe atom alone as assumed by Shannon.[32] Further, the bonded radii of the S atoms comprising the S_2 dimers in marcasite and pyrite are ∼0.1 Å smaller than the radii of the S atoms in troilite and smythite. Accordingly, the ED is more accumulated and locally concentrated at the bcp along the low-spin Fe−S bond paths. Given the low-spin state of the Fe atoms in pyrite and marcasite, the smaller radii of the Fe atoms are consistent with Xα calculations and spectroscopic studies used to model the bonded interactions for pyrite.[54]

The bonded radii of the Fe atoms in chalcopyrite and cubanite are both the same (1.07 Å), on average, consistent with the possibility that oxidation number of the Fe atom in cubanite is

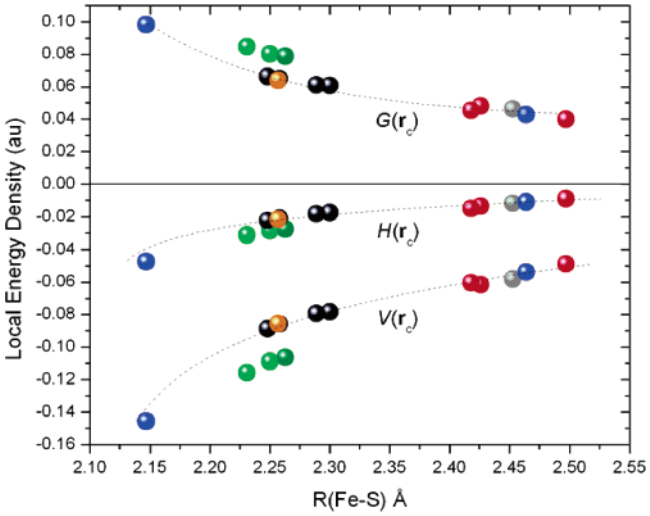

Figure 5. The local kinetic energy density, $G(\mathbf{r}_c)$, the local potential energy density, $V(\mathbf{r}_c)$, and the electron energy density, $H(\mathbf{r}_c)$, for the sulfides identified in the upper corner of Figure 4a plotted against the experimental Fe−S bond lengths, R(Fe−S).

close to being nominally trivalent as in chalcopyrite. The bonded radius of the tetrahedrally coordinated Fe atoms in greigite, however, is smaller yet (1.02 Å), consistent with the possibility that atom is nominally tetravalent. Tetravalent Fe is also consistent with the smaller size of the FeS_4 tetrahedra observed for greigite as compared with those observed for chalcopyrite and cubanite. The bonded radius of the Fe atom calculated for the H_4FeS_4 molecule is slightly smaller (1.00 Å) than that calculated for greigite (1.02 Å), whereas the calculated radius of the S atom (1.13 Å) is in exact agreement with that calculated for greigite.

Connection between the Experimental Fe−S Bond Lengths and the Local Energy Density Properties

The local kinetic energy density, $G(\mathbf{r}_c)$, and potential energy density at the bcp, $V(\mathbf{r}_c)$, of a bonded interaction are each connected to $\nabla^2\rho(\mathbf{r}_c)$ by the local form of the virial theorem $1/4\nabla^2\rho(\mathbf{r}_c) = 2G(\mathbf{r}_c) + V(\mathbf{r}_c)$.[55] For a geometry optimized minimum energy structure, the kinetic energy density, $G(\mathbf{r}_c)$, is always positive, and the local potential energy density $V(\mathbf{r}_c)$ is always negative. As displayed in Figure 5, with decreasing Fe−S bond length, $G(\mathbf{r}_c)$ increases and $V(\mathbf{r}_c)$ decreases at a faster rate such the local electronic energy density, $H(\mathbf{r}_c) = G(\mathbf{r}_c) + V(\mathbf{r}_c)$, is negative. As asserted by Cremer and Kraka,[56] $H(\mathbf{r}_c)$ can be used as a measure of the character of a bonded interaction. When it is positive and the local kinetic energy dominates, $G(\mathbf{r}_c) > |V(\mathbf{r}_c)|$, a bonded interaction is asserted to be a closed-shell interaction, and when it is negative and the local potential energy dominates, $|V(\mathbf{r}_c)| > G(\mathbf{r}_c)$, it is asserted to be a shared interaction. In general, the more negative is the value of $H(\mathbf{r}_c)$, the larger is the magnitude of $V(\mathbf{r}_c)$, and the smaller is the value of $G(\mathbf{r}_c)$, the greater is the shared character of the bonded interaction. The bonded interactions displayed in Figure 5 indicate that the shared character of the Fe−S bonded interactions increases for the high-spin Fe bonded interactions with decreasing bond length, coordination number, and the oxidation number of the Fe atom.[57] The low-spin Fe−S bonded interactions comprising the FeS_6 octahedra in pyrite and marcasite are indicated to have more shared character than the high-spin Fe−S interactions comprising the octahedra in troilite, smythite, and greigite. The fact that the $H(\mathbf{r}_c)$ values for the Fe−S bonded interactions in chalcopyrite are similar to those in cubanite suggests that the bonded interactions for the two are similar.

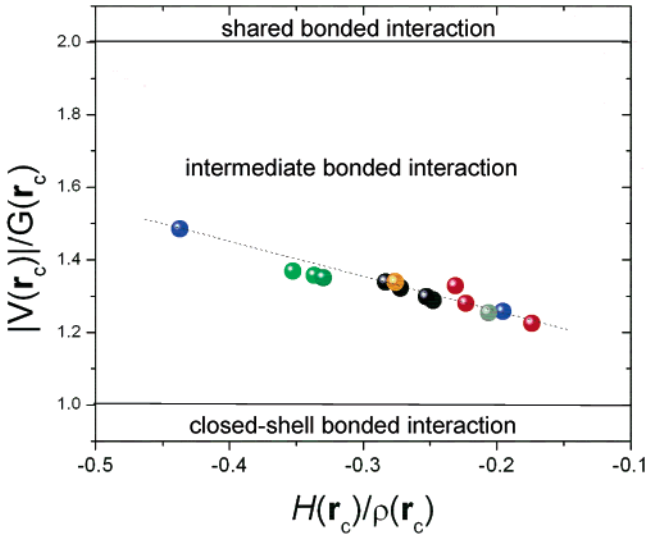

Figure 6. A scatter diagram of the bond index, $|V(\mathbf{r}_c)|/G(\mathbf{r}_c)$, defined by Espinosa et al.[58] plotted against the $H(\mathbf{r}_c)/\rho(\mathbf{r}_c)$ ratio for the sulfides defined in the upper right corner of Figure 4a.

Recently, Espinosa et al.[58] proposed a classification of bonded interactions based on the $|V(\mathbf{r}_c)|/G(\mathbf{r}_c)$ ratio. Bonded interactions with ratios less than 1 are indicated to be closed-shell interactions, those with ratios greater than 2 are indicated to be shared interactions, and those with ratios between 1 and 2 are indicated to be intermediate interactions. It was assumed that a bonded interaction is a closed-shell interaction when $H(\mathbf{r}_c) \geq 0$[56] and that it is a shared interaction when $\nabla^2\rho(\mathbf{r}_c) \leq 0$.[59] The condition $H(\mathbf{r}_c) = 0$ implies that $G(\mathbf{r}_c) + V(\mathbf{r}_c) = 0$, and, similarly, the condition that $\nabla^2\rho(\mathbf{r}_c) = 0$ implies that $2G(\mathbf{r}_c) + V(\mathbf{r}_c) = 0$ such that the two equalities $|V(\mathbf{r}_c)|/G(\mathbf{r}_c) = 1$ and $|V(\mathbf{r}_c)|/G(\mathbf{r}_c) = 2$ each hold, respectively. With these equalities, a bonded interaction is indicated to be a closed-shell when the ratio $|V(\mathbf{r}_c)|/G(\mathbf{r}_c) < 1$, shared when $|V(\mathbf{r}_c)|/G(\mathbf{r}_c) > 2$, and of intermediate character when the ratio falls between 1 and 2. The ratio $|V(\mathbf{r}_c)|/G(\mathbf{r}_c)$ is plotted against bond degree parameter $H(\mathbf{r}_c)/\rho(\mathbf{r}_c)$ in Figure 6 where the ratio ranges between ~1.2 and ~1.5 and the parameter is negative, a result that indicates that the Fe−S bonded interactions are intermediate in character between closed-shell and shared interactions. As found for a large number of oxides,[57] the shared character of the high-spin Fe−S bonds likewise increases with decreasing coordination number with the bonded interactions in the FeS_4 tetrahedra indicated to be more shared than those in the FeS_6 octahedra. Further, the octahedral low-spin Fe−S bonded interactions in pyrite and marcasite are indicated to be more shared interactions than those for the octahedral high-spin Fe−S interactions. Also, the bond degree ratio for the Fe−S interactions increases with the oxidation number of the Fe atom from 1.25 for divalent to 1.35 for trivalent to 1.45 for tetravalent Fe, with the bonded interaction in greigite indicated to be the most shared of the interactions. The ratios for the Ni−S interactions determined for the Ni-sulfides vaesite, millerite, and heazlewoodite show a similar but smaller range of values (1.20−1.26). As the Fe−S bonded interactions for trivalent and tetravalent Fe atoms display larger ratios, they are indicated to display a slightly greater component of shared character.

Net Atomic Charges

As defined by Bader,[55] an atom in a material consists of its nucleus and the associated basin of electrons, the ingredients of which are bounded by a surface $S(\mathbf{r})$ that exhibits the property

of zero flux, meaning that $S(\mathbf{r})$ is not crossed by any gradient vectors in $\rho(\mathbf{r})$. This condition is satisfied by the inner product $\nabla\rho(\mathbf{r})\cdot\mathbf{n}(\mathbf{r}) = 0\ \forall\ \mathbf{r} \in S(\mathbf{r})$, where $\mathbf{n}(\mathbf{r})$ is a unit vector oriented perpendicular to the surface at $\mathbf{r}$. As defined above, the electrons enclosed by $S(\mathbf{r})$ together with the nucleus collectively comprise the atom. By integrating the ED over the range of the atomic basin, the number of electrons in the basin is determined. The net charge of an atom is obtained by summing the nuclear charge of the atom and the electronic charge associated with the number of the electrons in the basin. On the basis of the volumes of the basins and the net atomic charges generated with TOPOND,[44] the following chemical formulas were found: marcasite, $Fe^{0.67+}S_2^{0.34-}$; pyrite, $Fe^{0.67+}S_2^{0.34-}$; troilite, $Fe^{0.81+}S^{0.81-}$; smythite, $Fe^{0.81+}Fe_2^{0.99+}S_2^{0.54-}S_2^{0.84-}$; cubanite, $Cu^{0.66+}(Fe^{0.85+})_2S^{0.77-}S_2^{0.79-}$; chalcopyrite, $Cu^{0.62+}Fe^{0.86+}S_2^{0.74-}$; greigite, $Fe^{0.93+}Fe_2^{1.03+}S_4^{0.75-}$. The charges conferred on the ^{IV}Fe atoms for cubanite and chalcopyrite are practically the same, whereas that conferred on the ^{IV}Fe atom for greigite is slightly larger (~10%). However, the charges calculated for the H_4FeS_4 molecule resulted in the formula $H_4^{0.02-}Fe^{0.88+}S_4^{0.20-}$ with a charge conferred on the Fe atom about the same as that on the Fe atoms in chalcopyrite and cubanite but smaller than that conferred on the atom in greigite. The similar charges conferred on the Fe atoms for both cubanite and chalcopyrite suggest that the oxidation number for the Fe atoms comprising the two is similar, whereas the larger charge on the Fe atom for greigite suggests that the oxidation number of the Fe atom is larger in greigite than it is in cubanite and chalcopyrite. However, as the atomic basins for a gas-phase molecule like H_4FeS_4 are of infinite dimensions and those for a crystal like greigite are finite, it is not clear to what extent the charges for the two systems can be compared.

The magnitude of the charges conferred on the Fe atoms in pyrite and marcasite is generally smaller than those conferred on the octahedrally coordinated Fe atoms in troilite, smythite, and greigite. As may be expected, the magnitude of the net charge on the S_2 dimers (−0.68 e) is also smaller than that on the S atoms in troilite and smythite (−0.75 e). The different net charges conferred on the two nonequivalent S atoms in smythite can be related to different environments of the two atoms. As observed above, smythite is a sheet structure consisting of neutral slabs of face-sharing FeS_6 octahedra, four S monolayers thick. The S atoms comprising the two interior monolayers are each bonded to six Fe atoms, while those comprising the surface monolayers are each bonded to three Fe atoms. The surface S atoms bonded to three Fe atoms have a net charge that is smaller (−0.54 e) in magnitude than the interior S atoms that are each bonded to six Fe atoms (−0.84 e). In addition, the charges conferred on the Fe atoms coordinated by the S atoms of the interior monolayers are smaller, 0.81+, in magnitude than those coordinated by the S atoms of the interior and surface monolayers (0.99+). In short, the magnitude of net atomic charges conferred on the Fe and S atoms both increase from the interior of the slab to the surface.

The $\rho(\mathbf{r}_c)$ values calculated for S−S bonded interactions comprising the S_2 dimers for the disulfides pyrite, marcasite, and vaesite are similar to those calculated for the S−S bonded interactions comprising the eight member S_8 rings of native sulfur (Figure 7). In addition to the two well-developed bond paths that connect neighboring S atoms in the ring, each S is connected to S atoms in adjacent rings by bond paths, the number ranging between three and six. Bond paths also exist between the surface S atoms of the slabs of FeS_6 octahedra for smythite, suggesting that the slabs are bonded together by S−S interactions (Figure 2d). The presence of a bond path linking a pair of atoms has been asserted to be a necessary and sufficient condition for the pair to be bonded.[24] Whether the pair is bonded in a chemical sense has been a subject of considerable debate, a debate that will not be resolved here. Nonetheless, as the ED of a material adopts a configuration wherein the energy of the resulting configuration is minimized, the accumulation of the ED along a bond path is therefore expected to have a stabilizing impact on a structure.[60,61]

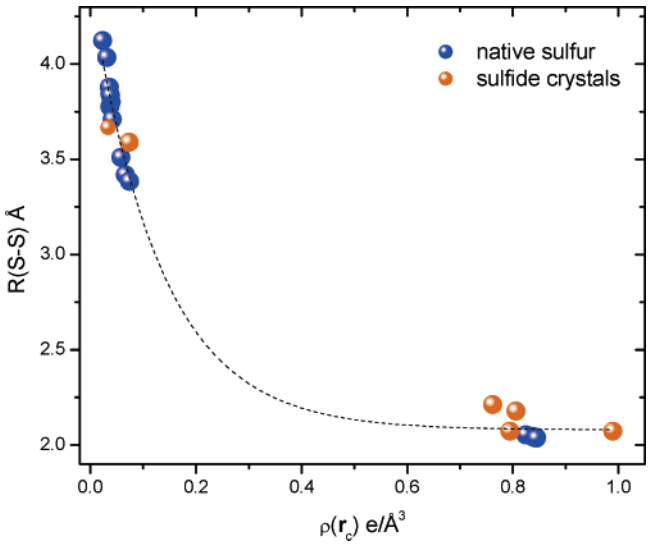

Figure 7. The S−S bond lengths, R(S−S), observed for native sulfur, smythite, heazlewoodite, marcasite, pyrite, vaesite, NiS_2, and covellite, CuS, plotted against the value of $\rho(\mathbf{r}_c)$. The native sulfur bonded interactions are plotted as blue spheres, and those for the sulfide crystals are plotted as orange spheres.

Concluding Remarks

The connection that exists between the Fe−S bond lengths and the bcp and the local energy density properties is similar to that established for the bonded interactions for a variety of non-transition metal oxides,[62] and for the Fe−O, Mn−O, Ni−O, and Co−O bonded interactions observed for a number of transition metal bearing oxides and organic structures.[63−66] On the basis of the theoretical bond critical properties and the net charges conferred on the Fe and Cu atoms in chalcopyrite together with spectroscopic evidence, it is concluded that the valences of Cu and Fe atoms in chalcopyrite are monovalent and trivalent, respectively. The Cu atom in cubanite is also monovalent and ordered at a single site, whereas Mössbauer evidence indicates that Fe^{2+} and Fe^{3+} are randomly distributed in a pair of tetrahedra. Yet, as observed above, the rms amplitudes for the Fe atoms are significantly smaller than that observed for the Cu atom, evidence that appears to contradict a disordered configuration Fe atoms. The observed bond length data and the calculated bond critical point properties support the proposal that the valence of the tetrahedral Fe atom comprising greigite is 4+, but the evidence is not conclusive. Nonetheless, the fact that the geometry optimized Fe−S bond length and the value of the ED at the bond critical for the H_4FeS_4 molecule is virtually the same as that for greigite suggests that the proposal merits consideration. Further, if the proposal were true, then it would explain why greigite has a limited stability with respect to pH, why it is difficult to synthesize, and its metastability.[67]

In a comparison of model multipole theoretical ED distributions and experimental distributions for several silicates determined with high-resolution and high-energy synchrotron single-

crystal diffraction data,[68,69] it was found that the theoretical distributions are in close agreement with the experimental distributions. The close agreement of the experimental and theoretical bond critical point properties reported for heazlewoodite by Spackman et al.[27] also indicates that the accuracy of theoretical model ED distribution rivals that of the experimental model. On the basis of these results, it is anticipated that the accuracy of the theoretical ED distributions for Fe and Cu sulfides together with their calculated bcp and local energy density properties will rival those of the experimental distributions.

Acknowledgment. The National Science Foundation and the U.S. Department of Energy are thanked for supporting this study in part with grants EAR-0609885 (N.L.R. and G.V.G.), EAR-0609906 (R.T.D.), and DE-FG02-97ER14751 (D.F.C.). K.M.R. acknowledges a grant from the U.S. Department of Energy (DOE), Office of Basic Energy Sciences, Engineering and Geosciences Division, and support from the Environmental Molecular Sciences Laboratory (EMSL) at the Pacific Northwest National Laboratory (PNNL). The computations were performed in part at the EMSL at PNNL. The EMSL is a national scientific user facility sponsored by the U.S. DOE's Office of Biological and Environmental Research. PNNL is operated by Battelle for the DOE under Contract DE-AC06-76RLO 1830. G.V.G. wishes to acknowledge the Gledden Foundation for generously supporting his visit to the University of Western Australia as a Gledden Senior Fellow where much of this paper was written. He also wishes to thank Virginia Tech for providing additional support for the visit. Finally, it is our pleasure to thank Professor David Vaughan for reviewing the manuscript and making a number of excellent suggestions that led to substantial improvements.

References and Notes

(1) Wuensch, B. J. Sulfide Crystal Chemistry. In *Reviews in Mineralogy*; Ribbe, P. H., Ed.; Mineralogical Society of America: Washington, DC, 1974; Vol. 1, p W1.

(2) Prewitt, C. T.; Rajamani, V. Electron Interactions and Chemical Bonding in Sulfides. In *Sulfide Crystal Chemistry*; Ribbe, P. H., Ed.; Mineralogical Society of America: Washington, DC, 1976; Vol. 1, p PR1.

(3) Tossell, J. A.; Vaughan, D. J. *Theoretical Geochemistry: Applications of Quantum Mechanics in the Earth and Mineral Sciences*; Oxford University Press Inc.: Oxford, 1992.

(4) Vaughan, D. J.; Craig, J. R. *Mineral Chemistry of Metal Sulfides*; Cambridge University Press: New York, 1978.

(5) Kostov, I. D.; Min<crn>ceva-Stefanova, J. *Sulphide Minerals: Crystal Chemistry, Parageneses, and Systematics*; E. Schweizerbart'sche Verlagsbuchhandlung: Stuttgart, 1982.

(6) Pauling, L. Historical Perspective. In *Structure and Bonding in Crystals*; O'Keeffe, M., Navrotsky, A., Eds.; Academic Press: New York, 1981; Vol. 1, p 1.

(7) Gibbs, G. V.; Downs, R. T.; Prewitt, C. T.; Rosso, K. M.; Ross, N. L.; Cox, D. F. *J. Phys. Chem. B* **2005**, *109*, 21788.

(8) Gibbs, G. V.; Cox, D. F.; Rosso, K. M.; Kirfel, A.; Lippmann, T.; Blaha, P.; Schwarz, K. *Phys. Chem. Miner.* **2005**, *32*, 114.

(9) Fleet, M. E. *Acta Crystallogr., Sect. B* **1972**, *28*, 1237.

(10) Martonak, R.; Donadio, D.; Oganov, A. R.; Parrinello, M. *Nat. Mater.* **2006**, *5*, 623.

(11) Pauling, L. *J. Am. Chem. Soc.* **1929**, *51*, 1010.

(12) Hoggins, J. T.; Steinfink, H. *Inorg. Chem.* **1976**, *15*, 1682.

(13) Brown, I. D.; Shannon, R. D. *Acta Crystallogr., Sect. A* **1973**, *29*, 266.

(14) Bragg, W. L. *Atomic Structure of Minerals*; Cornell University Press: Ithaca, NY, 1937.

(15) Liebau, F. *Structural Chemistry of Silicates: Structure, Bonding, and Classification*; Springer-Verlag: New York, 1985.

(16) O'Keeffe, M.; Brese, N. E. *J. Am. Chem. Soc.* **1991**, *113*, 3226.

(17) Mohri, F. *Acta Crystallogr., Sect. B* **2000**, *56*, 626.

(18) Stevens, E. D.; Delucia, M. L.; Coppens, P. *Inorg. Chem.* **1980**, *19*, 813.

(19) Serres, A. *J. Phys. Radium* **1953**, *14*, 689.

(20) Finklea, S. L.; Cathey, L.; Amma, E. L. *Acta Crystallogr., Sect. A* **1976**, *32*, 529.

(21) Zeng, Y.; Holzwarth, N. A. W. *Phys. Rev. B* **1994**, *50*, 8214.

(22) Aray, Y.; Rodriguez, J. *ChemPhysChem* **2001**, *2*, 599.

(23) Aray, Y.; Rodriguez, J.; Vega, D.; Rodriguez-Arias, E. N. *Angew. Chem., Int. Ed.* **2000**, *39*, 3810.

(24) Bader, R. F. W. *J. Phys. Chem. A* **1998**, *102*, 7314.

(25) Lu, Z. W.; Klein, B. M.; Singh, D. J. *Phys. Rev. B* **1996**, *54*, 13542.

(26) Kiehl, P.; Rohmer, M. M.; Benard, M. *Inorg. Chem.* **2004**, *43*, 3151.

(27) Spackman, M. A.; Gibbs, G. V.; Downs, R. T., in preparation.

(28) Koritsanszky, T. S.; Coppens, P. *Chem. Rev.* **2001**, *101*, 1583.

(29) Boekema, C.; Krupski, A. M.; Varasteh, M.; Parvin, K.; van Til, F.; van der Woude, F.; Sawatzky, G. A. *J. Magn. Magn. Mater.* **2004**, *272*−*76*, 559.

(30) Pearce, C. I.; Pattrick, R. A. D.; Vaughan, D. J.; Henderson, C. M. B.; van der Laan, G. *Geochim. Cosmochim. Acta* **2006**, *70*, 4635.

(31) Hall, S. R.; Stewart, J. M. *Acta Crystallogr., Sect. B* **1973**, *29*, 579.

(32) Shannon, R. D. Bond distances in sulfides and a preliminary table of sulfide crystal radii. In *Structure and Bonding in Crystals*; O'Keeffe, M., Navrotsky, A., Eds.; Academic Press: New York, 1981; Vol. 2, p 53.

(33) Greenwood, N. N.; Whitfield, H. J. *J. Chem. Soc. A* **1968**, 1697.

(34) Szymanski, J. T. *Z. Kristallogr.* **1974**, *149*, 218.

(35) McCammon, C. A.; Zhang, J.; Hazen, R. M.; Finger, L. W. *Am. Mineral.* **1992**, *77*, 937.

(36) Fleet, M. E. *Can. Mineral.* **1972**, *11*, 901.

(37) McCammon, C. A. *Am. Mineral.* **1995**, *80*, 1.

(38) Skinner, B. J.; Erd, R. C.; Grimaldi, F. S. *Am. Mineral.* **1964**, *49*, 543.

(39) Spender, M. R.; Coey, J. M. D.; Morrish, A. H. *Can. J. Phys.* **1972**, *50*, 2313.

(40) Hong, H. Y.; Steinfink, H. *J. Solid State Chem.* **1972**, *5*, 93.

(41) Rendon-Diazmiron, L. E.; Steinfink, H. *J. Solid State Chem.* **1979**, *27*, 261.

(42) Lemley, J. T.; Jenks, J. M.; Hoggins, J. T.; Eliezer, Z.; Steinfink, H. *J. Solid State Chem.* **1976**, *16*, 117.

(43) Saunders, V. R.; Dovesi, R.; Roetti, C.; Causa, M.; Harrison, N. M.; Orlando, R.; Apra, E. *CRYSTAL98 User's Manual*; University of Torino: Torino, Italy, 1998.

(44) Gatti, C. *TOPOND96 User's Manual*; CNR-CSRSRC: Milano, Italy, 1997.

(45) King, H. E.; Prewitt, C. T. *Acta Crystallogr., Sect. B* **1982**, *38*, 1877.

(46) Paszkowicz, W.; Leiro, J. A. *J. Alloys Compd.* **2005**, *401*, 289.

(47) Wijeyesekera, S. D.; Hoffmann, R. *Inorg. Chem.* **1983**, *22*, 3287.

(48) Erd, R. C.; Evans, H. T., Jr.; Richter, D. H. *Am. Mineral.* **1957**, *42*, 309.

(49) Dirac, P. A. M. *The Principles of Quantum Mechanics*; Oxford University Press: Oxford, UK, 1958.

(50) Vosko, S. H.; Wilk, L.; Nusair, M. *Can. J. Phys.* **1980**, *58*, 1200.

(51) Towler, M. D.; Dovesi, R.; Saunders, V. R. *Phys. Rev. B* **1995**, *52*, 10150.

(52) Lichanot, A.; Apra, E.; Dovesi, R. *Phys. Status Solidi B* **1993**, *177*, 157.

(53) Gibbs, G. V.; Jayatilaka, D.; Spackman, M. A.; Cox, D. F.; Rosso, K. M. *J. Phys. Chem. A* **2006**, *110*, 12678.

(54) Vaughan, D. J.; Tossell, J. A. *Phys. Chem. Miner.* **1983**, *9*, 253.

(55) Bader, R. F. W. *Atoms in Molecules*; Oxford Science Publications: Oxford, UK, 1990.

(56) Cremer, D.; Kraka, E. *Croat. Chem. Acta* **1984**, *57*, 1259.

(57) Mooser, E.; Pearson, W. B. *Acta Crystallogr.* **1959**, *12*, 1015.

(58) Espinosa, E.; Alkorta, I.; Elguero, J.; Molins, E. *J. Chem. Phys.* **2002**, *117*, 5529.

(59) Bader, R. F. W.; Essen, H. *J. Chem. Phys.* **1984**, *80*, 1943.

(60) Gatti, C. *Z. Kristallogr.* **2005**, *220*, 399.

(61) Gatti, C. *Z. Kristallogr.* **2005**, *220*, 399.

(62) Gibbs, G. V.; Cox, D. F.; Crawford, T. D.; Rosso, K. M.; Ross, N. L.; Downs, R. T. *J. Chem. Phys.* **2006**, 084704.

(63) Marabello, D.; Bianchi, R.; Gervasio, G.; Cargnoni, F. *Acta Crystallogr., Sect. A* **2004**, *A60*, 494.

(64) Bianchi, R.; Gatti, C.; Adovasio, V.; Nardelli, M. *Acta Crystallogr., Sect. B* **1996**, *52*, 471.

(65) Poulsen, R. D.; Bentien, A.; Graber, T.; Iversen, B. B. *Acta Crystallogr., Sect. A* **2004**, *60*, 382.

(66) Overgaard, J.; Larsen, F. K.; Schiott, B.; Iversen, B. B. *J. Am. Chem. Soc.* **2003**, *125*, 11088.

(67) Chen, X. Y.; Zhang, X. F.; Wan, J. X.; Wang, Z. H.; Qian, Y. T. *Chem. Phys. Lett.* **2005**, *403*, 396.

(68) Gibbs, G. V.; Whitten, A. E.; Spackman, M. A.; Stimpfl, M.; Downs, R. T.; Carducci, M. D. *J. Phys. Chem. B* **2003**, *107*, 12996.

(69) Kirfel, A.; Lippmann, T.; Blaha, P.; Schwarz, K.; Cox, D. F.; Rosso, K. M.; Gibbs, G. V. *Phys. Chem. Miner.* **2005**, *32*, 301.